Wind-Induced Error of Raindrop Size Distribution Measurement Using a Two-Dimensional Video Disdrometer

VLADISLAV NEŠPOR, WITOLD F. KRAJEWSKI, AND ANTON KRUGER

Iowa Institute of Hydraulic Research, University of Iowa, Iowa City, Iowa

(Manuscript received 9 August 1999, in final form 20 January 2000)

ABSTRACT

The authors investigate a disdrometer that provides information on raindrop size distribution, terminal velocity, and shape using video imaging technology. Two video cameras are enclosed in a large box and provide images of the passing drops. The box modifies the air flow, and this in turn affects the drop trajectories, causing some of the drops to miss the sensing area in the instrument's opening. The authors investigate the distortion of the trajectories using numerical simulation methods of computational fluid dynamics. This approach enables the authors to quantify the effects of wind velocity and direction on the instrument's measurement of drop size distribution. The results of the study lead to the conclusion that the shape of the enclosure of the instrument causes errors in the detection of the small drops. Small drops can get caught in a vortex that develops over the inlet. Some of them end up being counted more than once as they cross the sensing area while others are carried away and not counted at all. Also, the spatial distribution of the drops passing across the sensing area is distorted by the wind. The computational results are supported by observational evidence.

1. Introduction

The influence of wind on the measurement accuracy of rainfall characteristics, such as intensity (mm h^{-1}) and accumulation (mm) using a rain gauge, is widely acknowledged. Numerous investigators attempted to quantify the uncertainty of the wind effect (Larson and Peck 1974; Legates and DeLiberty 1993; Yang et al. 1998; Sevruk and Hamon 1984; Nešpor and Sevruk 1999). Most of these studies were performed as field experiments, and error evaluations were done by comparing the measurements of a given gauge design against a reference standard, usually a pit gauge. The main reason why wind affects the gauge observations of rainfall is the fact that the gauge is an elevated structure that forces the air to flow around it. This, in turn, modifies the trajectories of the falling raindrops and causes some of them to miss the gauge orifice.

Recently, a new device became available for measuring rainfall characteristics. The device is the two-dimensional video disdrometer developed by Joanneum Research.[1] The instrument is capable of recording images of each raindrop passing through the sensing area, and consequently, it provides information on raindrop size distribution (DSD), velocity, and shape. This information is important for many research applications, particularly for studies of radar remote sensing of rainfall. From drop size distribution, one can easily derive radar reflectivity, rainfall rate, attenuation, etc. From the drop shapes, additional variables, such as reflectivity at different polarizations and differential phase shift, can be calculated.

Our objective in this paper is to present the results of a computational study that indicates that wind may affect the raindrop observations collected by the two-dimensional video disdrometer (Fig. 1). The disdrometer is larger in size than most operational rain gauges, but it collects raindrops in a similar fashion, that is, by catching them into a funnel-like bucket in which the optical sensors are located. Therefore, it is reasonable to expect that the body of the instrument modifies the airflow and thus affects the drop trajectories. We describe the computational methodology used to quantify the wind effect on the disdrometer's measurement of the drop size distribution and complement the computational results with supporting empirical evidence. The results of our study should be useful to the research community, as several groups in the United States and elsewhere purchased the instrument and are using it to collect data in field experiments.

2. The disdrometer

The two-dimensional video disdrometer, designed and manufactured by Joanneum Research in Austria,

[1] Joanneum Research Institute of Applied Systems Technology, Inffeldgasse 12, A-8010 Graz, Austria; www.distrometer.at.

Corresponding author address: Witold Krajewski, Iowa Institute of Hydraulic Research, University of Iowa, Iowa City, IA 52242. E-mail: iihr@uiowa.edu

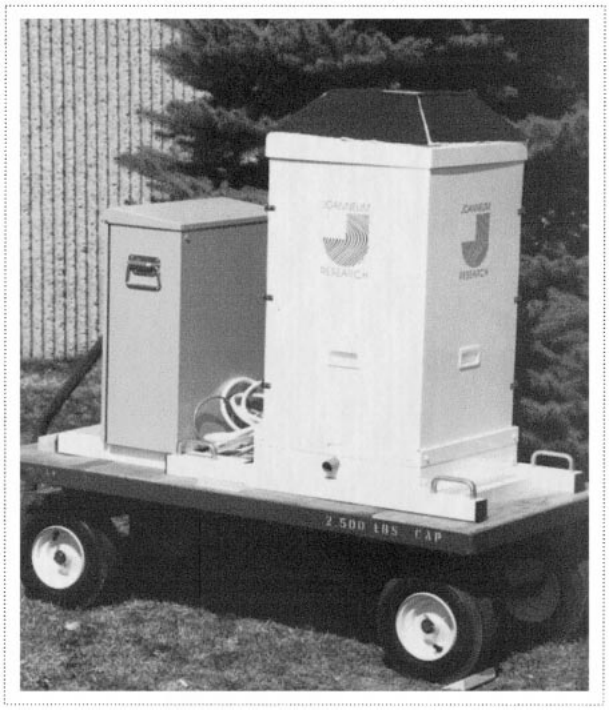

FIG. 1. The two-dimensional video disdrometer.

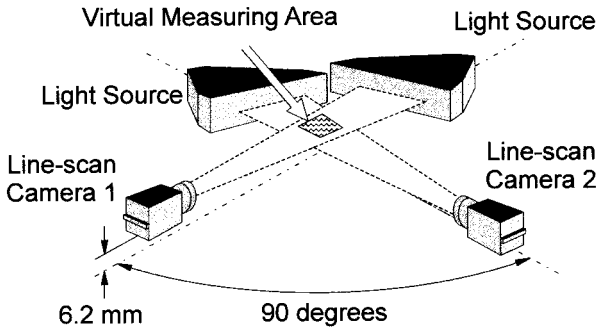

FIG. 3. The two-dimensional video disdrometer principle of operation.

was installed at the Iowa Institute of Hydraulic Research (IIHR) in 1996. This new instrument, specially designed for drop size distribution and shape measurements, has been used to collect data from some 50 storms in Iowa City, Iowa, as well as in NASA–sponsored field experiments in Florida and Brazil.

The instrument consists of several units. The main sensor is a unit with a rectangular base of 0.48 m × 0.48 m, positioned on the ground or a low platform (Fig. 1). The unit is 0.96 m high, inclined, and opened at the top. The orifice is a 0.25 m × 0.25 m square. The measuring area is inside the unit, approximately 0.08 m below the orifice level (Fig. 2).

Figure 3 depicts the principle of operation of the instrument. The intersection of two orthogonal horizontal light sheets forms the effective sensing area. As raindrops fall through the light sheets, they cast a shadow that is recorded by the line-scan cameras. Drop sizes and shapes are recovered in software. The operation is similar to flatbed scanners, and a more detailed description can be found in Krajewski et al. (1998). The light sheets are offset, enabling the measurement of vertical velocities. The nominal size of the measuring area is 0.1 m × 0.1 m.

Similar to can-type precipitation gauges, the disdrometer orifice is elevated above the ground, and the body of the measuring unit is exposed to the wind. As a consequence, the air is deviated around the unit and

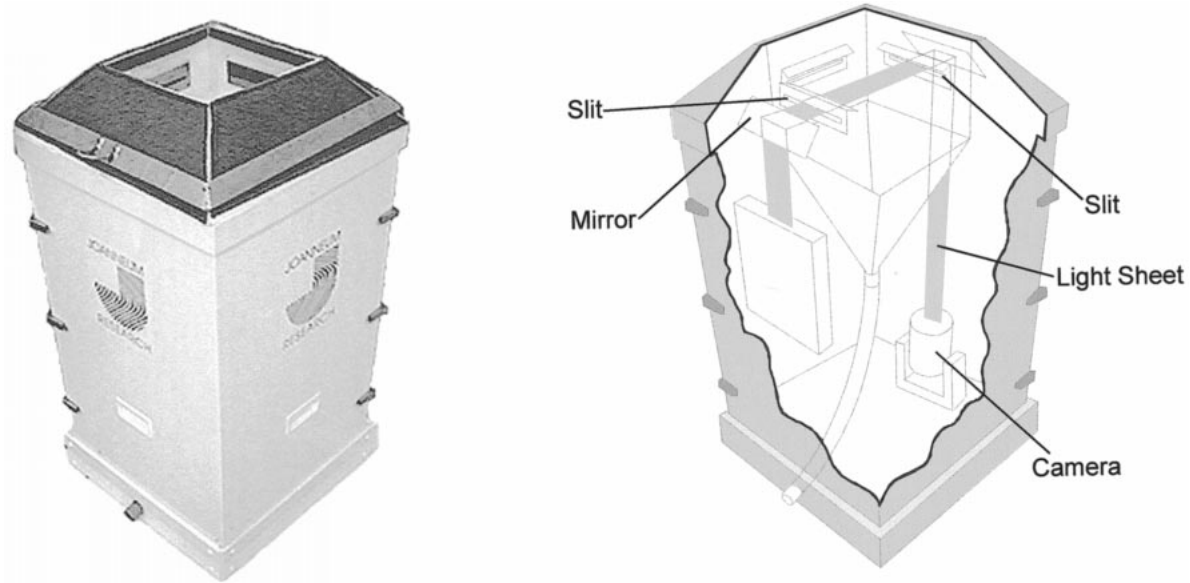

FIG. 2. The two-dimensional video disdrometer sensing area.

accelerated over its top, and an inner vortex is formed inside the disdrometer's opening. In contrast to cylindrical precipitation gauges, the airflow deformation depends on the reference angle—the horizontal angle between the free-stream (wind) velocity vector and the normal to the vertical disdrometer wall. The objective of the present work is to investigate the change of rain particle trajectories due to the wind field deformation and to estimate the resulting measurement error. We define the partial measurement error as the difference between the number of drops of a given size detected by the device and all the drops of that size that would have been detected if there was no wind effect. The total error is simply an integral of the partial errors across the DSD.

3. Methodology

The basic methods used in the present study are the same as in Nešpor and Sevruk (1999). Therefore, only a short description is presented here. The assessment of the wind-induced error is divided into two steps. In the first step, we computed three-dimensional airflow fields around the disdrometer body, and in the second step, we used the computed fields for the simulation of drop trajectories.

The computations of the airflow were carried out using the computational fluid dynamics (CFD) code PHOENICS (Version 2.2.1). The discretization method used in PHOENICS is based on the control-volume formulation. Because of the rectangular shape of the disdrometer body, we selected the Cartesian coordinate system with the z axis identical to the central vertical axis of the instrument. The extent of the computational domain was 1.69 m above and to each side of the disdrometer. The domain was discretized by a nonuniform grid with 80 cells in the vertical and 100 cells in both horizontal directions. The density of the grid was higher inside and close to the walls of the disdrometer. The disdrometer body was represented by totally blocking selected faces and volumes of the grid cells. The computational grid is shown in Fig. 4.

For the flow computation, we selected the k–ϵ turbulence model with the standard values of coefficients (Launder and Spalding 1974) built in PHOENICS. The inflow boundary conditions were simplified: the pressure was fixed to zero, and we assumed a vertical profile of turbulence quantities and free-stream velocity magnitude constant with height. The values of turbulence quantities at the inflow were derived from the turbulence intensity, which was set to 0.03, and from the turbulent kinematic viscosity, which was set to equal the kinematic viscosity of the air (see Nešpor and Sevruk 1999).

For the drop trajectory computation, we used the Lagrangian formulation, and we followed the procedure explained in more detail in Nešpor and Sevruk (1999). Because the density of the water is much higher than the density of the air, we considered only the Stokes drag force and ignored other forces acting on the particle surface (see, e.g., Hinze 1975). The drop drag coefficient was determined from the particle Reynolds number using the drag curve for water drops falling in the stagnant air (Beard 1977). To take into account the influence of turbulence on drop movement, a simplified model was applied. In this model, the particle Reynolds number was modified by replacing the laminar kinematic viscosity by the sum of the laminar and turbulent kinematic viscosities. This resulted in a modification of the particle drag coefficient. The model proved to give realistic estimates of wind-induced errors for cylindrical precipitation gauges, but its applicability is limited to flow fields computed using the present inflow conditions (Nešpor and Sevruk 1999).

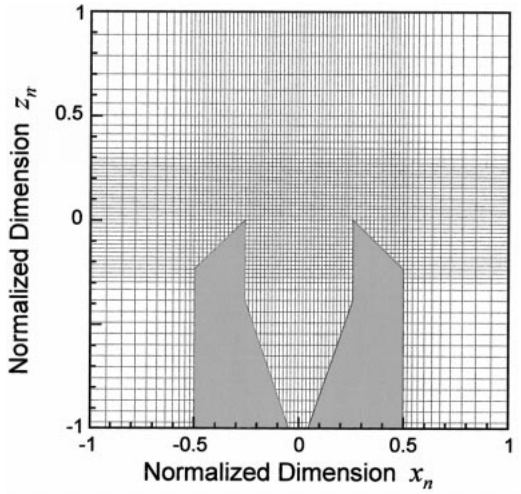

FIG. 4. The computational grid used for simulating the airflow around the disdrometer in the vicinity of its orifice. The dimensions are normalized by the size of the rectangular disdrometer base.

For a given drop diameter and wind velocity, we determined the trajectory by computing changes in the particle position in a stepwise manner. The local air velocities and turbulence quantities were determined from the computed flow fields. Similar to Nešpor and Sevruk (1999), we estimated the partial wind-induced error, the error for a given wind velocity and drops with a unique drop diameter, by computing the transformation of a horizontal rectangular grid from the undisturbed flow at the upper boundary of the computational domain. The transformation was defined by drop trajectories starting from the nodes of the original grid in the undisturbed flow. The nodes of the transformed grid were determined by intersections of trajectories with horizontal planes at the level with the orifice for intersections outside the disdrometer and at the level of the measuring area for intersections inside the disdrometer. The partial efficiency of the instrument was evaluated as a ratio of the area of the transformed grid inside the measuring area to the total size of the measuring area.

4. Results

a. Computations

We computed three-dimensional airflow fields around the disdrometer for combinations of nine wind velocities ranging between 1 and 12 m s^{-1} and six reference angles between 0° and 45°. The results reveal a complex nature of the flow inside and outside of the disdrometer. The flow is divided into the main flow outside (around) and recirculating flow inside the device. The flow patterns significantly depend on the reference angle. For the 0° and 45° angles, the flow is symmetrical with the vertical plane of symmetry parallel with the flow, and it is asymmetrical for other angles.

In Figs. 5 and 6, there are examples of computed flow fields for the 0° and 18° angles and free-stream wind velocity of 3 m s^{-1}. The plots in Fig. 5 are in the vertical plane perpendicular to the windward disdrometer wall and going through the center of the instrument. For the flow reference angle of 0°, this plane is identical with the plane of symmetry. The plots in Fig. 6 are in the horizontal plane at the level of the disdrometer orifice.

The velocity vectors in Fig. 5 top reveal that the core of the inner vortex is located approximately at the orifice level and above the measuring area, indicated by two dashed lines below the orifice. In the horizontal plane (Fig. 6 top) the velocity vectors inside the instrument show directions towards the vortex core. For the reference angle of 0°, the vortex core is in the plane of symmetry, and for the 18° angle, it is slightly shifted in the flow direction.

The magnitude of the velocity vector component perpendicular to the vertical plane of the plot is shown in Fig. 5 middle. For the reference angle of 0° (symmetrical case), there are only small deviations from zero velocity, caused by rounding errors in the computations. On the other hand, the case with the reference angle of 18° shows a reversed flow (negative values) deep inside and in the lee of the instrument.

Similar to Fig. 5 middle, Fig. 6 middle shows the magnitude of the vertical velocity vector component, which is perpendicular to the horizontal plane of the plot (the vertical velocity component). In the front windward part of the instrument at the orifice level, the flow is directed upward (positive values), and in the lee of the device, it is directed downward (negative values). In the recirculating flow inside the disdrometer, there are both positive and negative values of the vertical velocity magnitude. For the reference angle of 0°, the plot is symmetrical, whereas for the 18° angle, the negative values inside the instrument are moved in the flow direction to the inner corner of the catch area (Fig. 6 middle right).

Contour lines of normalized turbulent kinetic energy in Fig. 5 bottom reveal that the turbulence production is highest in the shear layer above the orifice. In the horizontal plane at the orifice level (Fig. 6 bottom) the highest values inside the catch area are in the regions with a negative vertical velocity vector component, partly because of the transport of the normalized turbulent kinetic energy from the shear layer above the instrument.

The flow regions with the highest influence on the particle trajectories are inside and behind the body of the disdrometer. In these regions, because of large vortexes, the turbulence level is high, and particles tend to follow the flow more closely. This effect is larger for smaller drops. Therefore, the trajectories of small drops are significantly influenced before they pass the measuring area. For certain combinations of the wind velocity, drop diameter, and reference flow angle, some drops enter the disdrometer and are caught by the inner vortex. The results of numerical simulation reveal that in extreme cases, raindrops can again leave the disdrometer without intersecting the measuring area or they can intersect this area more than once. In addition, the highly turbulent reverse flow behind the leeward side of the rim seems to cause some drops already behind the orifice to enter the disdrometer. Although these extreme cases of drop trajectories are difficult to confirm by observation and they can be significantly influenced by simplifications in the numerical simulation, they indicate that the influence of the flow field deformation above and inside the catch area could be very complex. Figure 7 shows an example of complex drop trajectories simulated in the computed flow field. They are simulated in the plane of symmetry for the reference angle of $\alpha = 0°$, wind velocity $v_f = 3$ m s^{-1}, and drop diameter $D = 1$ mm.

As demonstrated by the results of our simulations, there are several different effects contributing to the measurement error of the disdrometer. For low wind velocities and large drops, intersections of the drop trajectories with the plane level of the measuring area inside the disdrometer have almost the same distances as the nodal points of the original grid. They cover the entire measuring area, and the partial measurement error (i.e., error of detecting drops of a certain size) is negligible. However, already present is a shadowing effect of the disdrometer walls. The large drops (say, over 2 mm in diameter) enter the orifice with incident angle determined by the terminal and free-stream velocities. (This angle is 0° when there is no wind, and it increases as the wind velocity increases.) As a consequence, in the area adjacent to the inner windward walls, no drops intersecting the plane of the sensors can be observed. With increasing wind velocity and decreasing drop diameter the shadow area becomes larger, and eventually, it can intersect the measuring area contributing to the measurement error.

For smaller drops, similar to the results for precipitation gauges (Nešpor and Sevruk 1999), trajectories are significantly influenced by the accelerated external flow and turbulence in the shear layer. At the orifice level, drops are redistributed, and the horizontal distances between them are larger compared to the original grid in

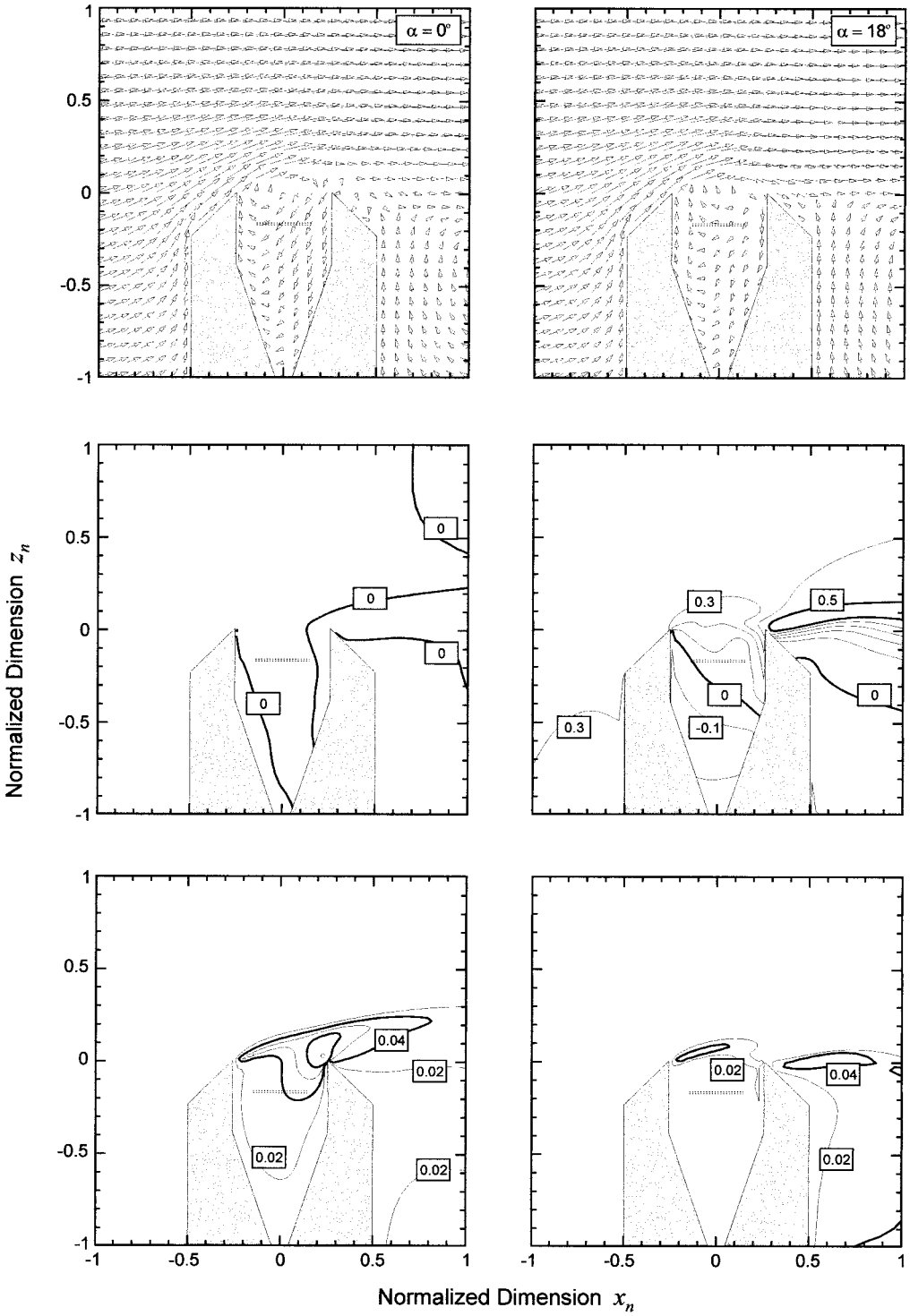

FIG. 5. Computed flow fields for reference angles $\alpha = 0°$ and $\alpha = 18°$ and free-stream wind velocity $v_f = 3$ m s^{-1} in the vertical plane perpendicular to the windward disdrometer wall and going through the gauge center. (top) Velocity vectors, (middle) the normalized magnitude of the velocity component perpendicular to the plane of plot, and (bottom) the normalized turbulent kinetic energy. The velocity magnitudes are normalized by v_f, the values of turbulent kinetic energy by v_f^2, and the dimensions are normalized by the size of the rectangular disdrometer base.

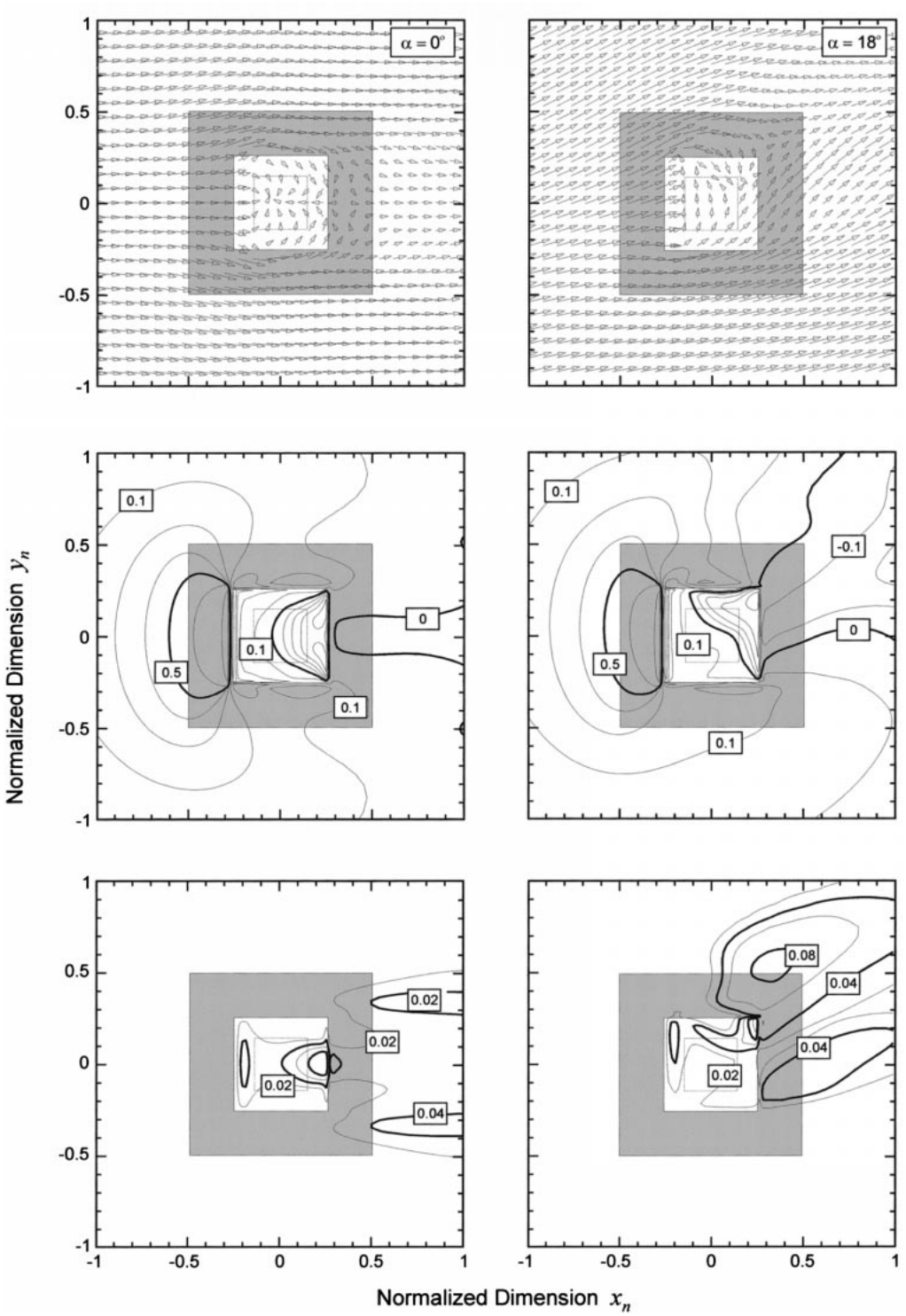

FIG. 6. The same as Fig. 5 but in the horizontal plane of the disdrometer orifice level.

the undisturbed flow above the disdrometer. As a result, a lower number of drops enter the device. Drops with very small diameters are blown away to the lee of the catch area and do not enter the orifice at all.

Another source of the measurement error results from the redistribution of drops by the flow inside the orifice. The inner vortex, which is above the measuring area, is characterized by the lateral flow toward its center

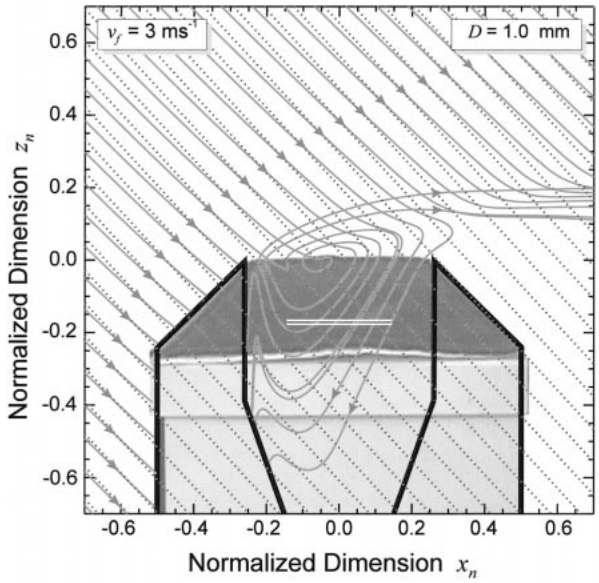

FIG. 7. Simulated drop trajectories for the reference angle of $\alpha = 0°$, wind velocity of $v_f = 3$ m s^{-1}, and the drop diameter of $D = 1$ mm. The trajectories are plotted in the vertical plane of symmetry. The dotted lines represent the undisturbed trajectories and the solid lines represent the trajectories in the airflow modified by presence of the disdrometer.

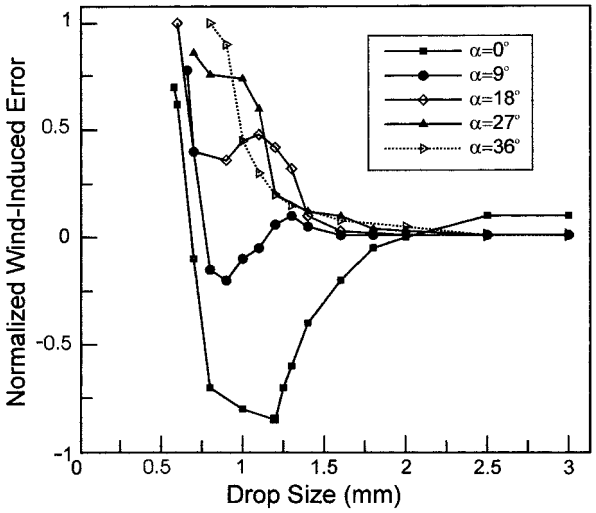

FIG. 9. Wind-induced partial measurement errors for different reference angles (wind directions) for the wind speed of 3 m s^{-1}. Positive errors imply missing (undetected) drops, negative errors imply drops counted more than once.

along the axis of vortex rotation and by the outward lateral flow at the outer vortex surface. Drops passing the inner vortex are laterally shifted in the vortex core toward the center and outside the vortex core toward the walls of the catch area. These effects significantly depend on the wind speed, drop diameter, and reference angle. Results of the computation reveal that the lateral shift of drops toward the center can increase the measurement efficiency by collecting drops from the margins of measuring area while the shift of drops toward the walls decreases the measurement efficiency.

Figure 8 shows examples of drop intersections with horizontal planes at the level of a) the orifice for drops outside the device and b) the measuring area for drops inside the catch area. The computations were carried out for the wind speed of 3 m s^{-1}, drop diameter of 1.2 mm, and reference angles of 0° and 18°. For the angle of 0° (Fig. 8a), drops are more concentrated in the center of measuring area. In this case, the numerical simulation predicts the measurement efficiency as high as 183% (the partial error is −83%). For the angle of 18° (Fig. 8b), the result is quite different. Drops are shifted toward the walls, out of the measuring area, and the measurement efficiency is 57% (the error is 43%).

In Fig. 9, partial measurement errors for different reference angles are shown as functions of the drop diameter. The values are computed for the wind speed of 3 m s^{-1}. The results indicate that the effect of drop

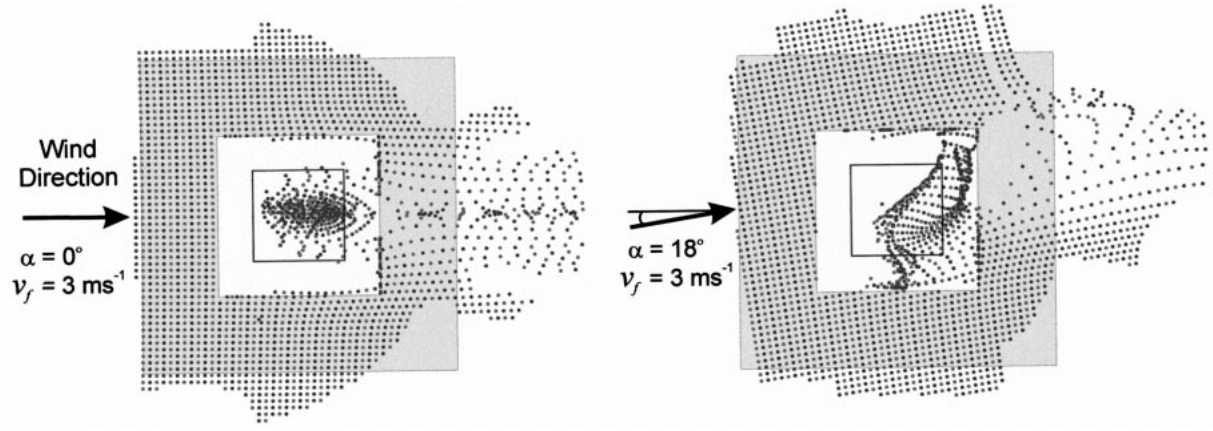

FIG. 8. Drop intersections with the horizontal planes at the level of the gauge orifice for drops outside the gauge and the measuring area for drops inside the gauge. The shown intersections are for the case of (a) $\alpha = 0°$ and (b) $\alpha = 18°$ angles, the wind velocity of $v_f = 3$ m s^{-1}, and the drop diameter of $D = 1.2$ mm.

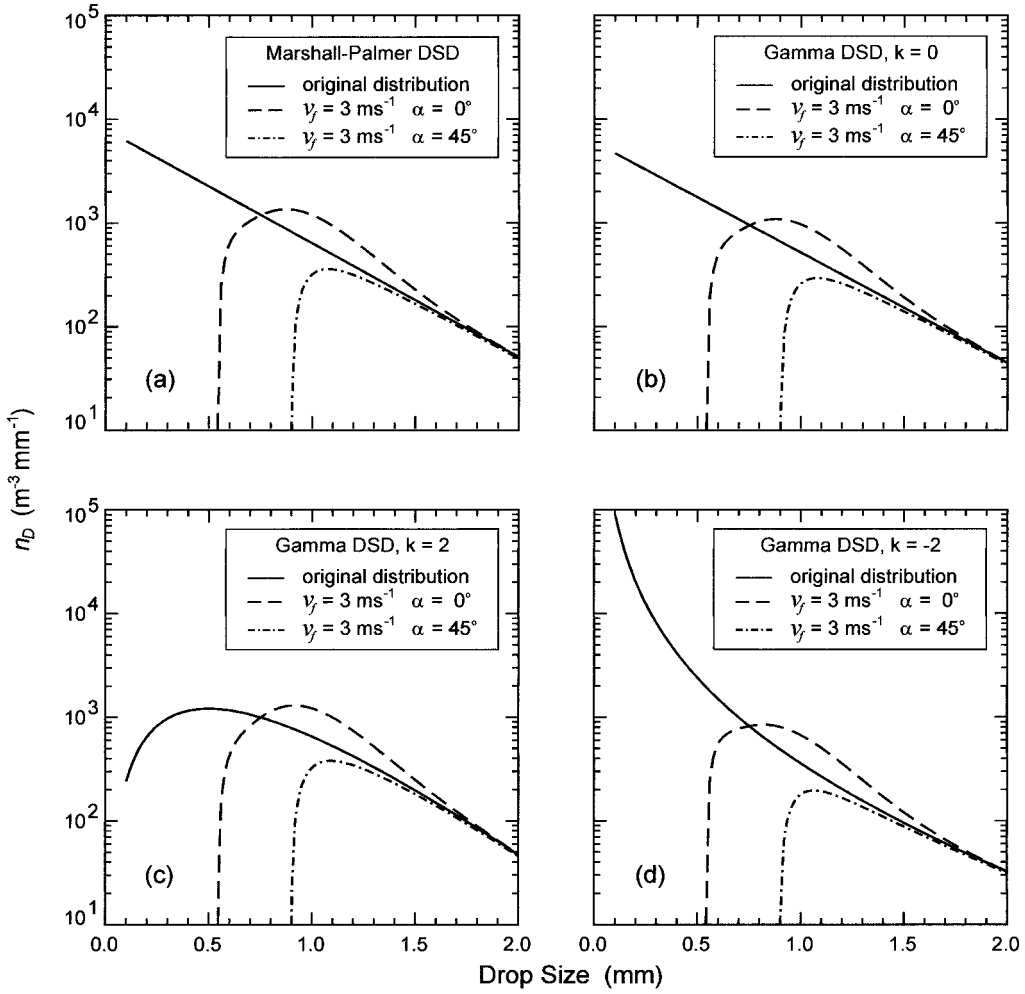

FIG. 10. Estimated modifications of DSD detected by the disdrometer for $v_f = 3$ m s^{-1} and $\alpha = 0°$ (dashed line) and $\alpha = 45°$ (dotted line) angles. The original distribution (solid line) corresponds to a rainfall rate of 10 mm h^{-1} and the (a) Marshall and Palmer DSD; (b) gamma DSD with parameter $k = 0$, (c) gamma DSD with $k = 2$, and (d) gamma DSD with $k = 2$. For definition and interpretation of k, see Ulbrich (1983).

concentration by inner vortex into the measuring area decrease with increasing reference angle. This effect is dominant for small angles (0° and 9°) and drop diameters between approximately 0.8 and 1.2 mm, causing negative measurement errors. For larger angles and smaller drops, other positive contributions to the error seem to prevail. For drops smaller than a certain limit, which depends on the reference angle, the measurement error is 100%. In other words, these small diameters would be missing in drop size spectra resulting from the disdrometer observations.

Let us consider a hypothetical example of the influence of estimated wind-induced errors on the resulting shape of DSD. Assume that the true DSD is based on the Marshall and Palmer distribution (Marshall and Palmer 1948) for the rate of rainfall $R = 10$ mm h^{-1}. We computed the errors of measuring this DSD using our disdrometer, with the constant wind velocity of 3 m s^{-1} and wind direction that corresponds to reference angles $\alpha = 0°$ and $\alpha = 45°$. We performed similar calculations for the gamma distribution (Ulbrich 1983). The results (Fig. 10) show that the number of drops per unit volume of air and unit drop size interval, n_D, deviates from the original distribution for drop sizes below approximately 2 mm, and this deviation depends on the reference angle. According to the computational results, drops with diameters below a certain limit, which also depends on the reference angle, would not be detected by the disdrometer at all. This is not quite valid for natural conditions because of fluctuations of the wind velocity vector.

b. Empirical observations

To qualitatively validate the computational results, we analyzed data collected from five storms that occurred

TABLE 1. Storms selected for the qualitative analysis.

Date	Duration (h)	Total rainfall accumulation (mm)	Number of drops collected
17 Aug 1997	8	10.6	395 303
28 May 1998	1	5.5	39 099
29 May 1998	3	3.6	36 036
20 Jun 1998	2	5.4	58 021
6 Jul 1998	2	11.1	142 593

during 1997 and 1998 in Iowa City, Iowa. The storms are summarized in Table 1. We used drop size information obtained using the video disdrometer as well as wind speed and direction from a high-resolution anemometer. The anemometer was located about 12 m away from the disdrometer; clocks of both instruments were carefully synchronized. The goal of our analysis was to check the spatial distribution (within the sensing area) of the drops of a selected size for the wind events with a certain velocity. If the observed patterns qualitatively agree with the results of the computations presented above, this would provide support for our numerical approach.

The disdrometer provides the arrival time (within a few milliseconds) for individual drops. First, we selected drops that arrived at the disdrometer during a time when the horizontal wind speed was in the range of 1.5–3.5 m s^{-1} (scaled down to the disdrometer orifice level), as follows. At 1.5 m s^{-1}, the air needs 12/1.5 = 8 s to travel 12 m between the anemometer and disdrometer. Thus, if the measured wind speed (at the anemometer) was in the range of 1.5–2.5 m s^{-1} for at least 8 s before and after a drop's arrival at the anemometer, we assumed the wind speed was in this range at the disdrometer. In addition, we required that the wind reference angle lies in the range of 25°–50°. Of the drops that remained, only drops with diameters in the range of 0.5–0.95 mm were retained. Of the original 671 052 drops, only 60 drops passed the three selection criteria. Figure 11 is a plan view of the disdrometer measuring area, showing the arrival position of these 60 drops. The spatial distribution is clearly skewed, and the drops tend to cluster in one corner and along one side, very much like in the corresponding calculations based on the CFD approach (see Fig. 6 for the corresponding flow patterns).

It may be surprising to some that only 0.01% of all drops satisfied our analysis criteria. However, this small number becomes more understandable if one considers that the wind was not significant for most of the selected events, that the selected angle sector is only a fraction of all the directions, and that the drop size range selected is only a fraction of the drop size spectrum. The above results led us to the conclusion that the numerical simulation of the wind effects has merit, even for the very complex geometry of the flow patterns around and inside of the 2D video disdrometer.

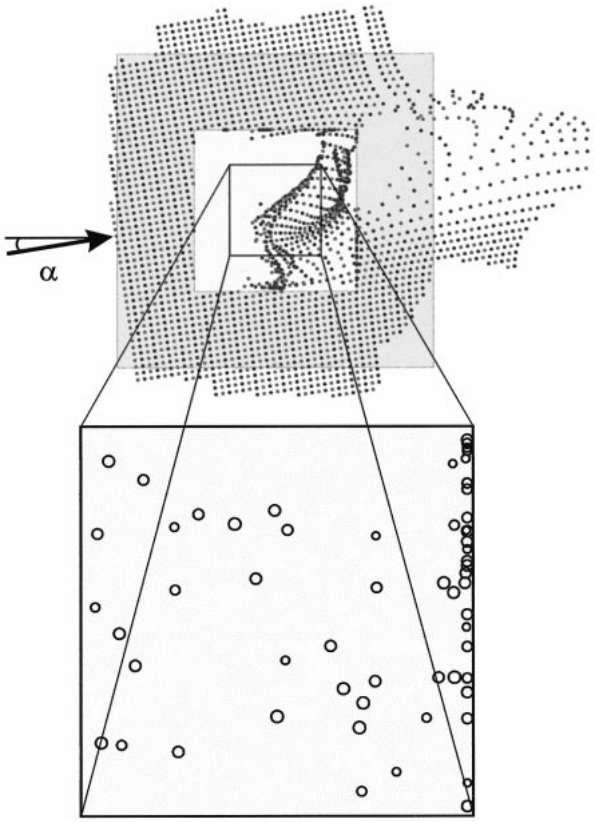

FIG. 11. Plan view of the disdrometer showing the arrival locations of 60 drops selected from an ensemble of some 670 000 raindrops. Drop diameters are not drawn to scale.

5. Conclusions

The results of our study reveal a large influence of the flow field deformation around the disdrometer body on raindrop trajectories. Trajectories of smaller drops are deflected before they reach the device opening. Also, the turbulence in the shear layer above the orifice and the inner vortex above the measuring area cause major deviations of the drop trajectories. The partial measurement error depends on the wind speed, drop diameter, and, because of the rectangular horizontal cross section of the instrument body, also on the reference angle (the wind direction).

Our computations indicate that the magnitude of the error can be negative (the instrument's efficiency is more than 100%) or positive (the efficiency is less than 100%). For very small drop diameters, depending on the reference angle, the partial measurement error is as high as 100%. In this case, the drops either enter the device and are all deflected by the inner vortex out of the measuring area or they do not enter the catch area at all. The computational results also indicate that under

certain conditions, drops can circulate inside the device, possibly intersecting the measuring area more than once.

The results, especially inside the device, are strongly influenced by the model that was chosen to take turbulence into account in drop trajectory computation. As comparative measurement data are not available, it is difficult to decide if these results are also quantitatively correct. In spite of that, the computations reveal the difficulties of measurement of raindrop size distribution using the two-dimensional video disdrometer.

We continue our investigation of the quantitative aspects of the measurement errors with a goal of developing a correction formula. The research proceeds along two major directions. First, we continue exploring the computational approach and its validation through specially designed experiments that involve wind tunnels and the particle image velocimetry (PIV) techniques (Fujita et al. 1998). Second, we have already investigated a different design of the instrument's enclosure and performed preliminary computations that indicate that a different shape of the orifice could mitigate adverse effects of the wind (Habib 1999). We will report the results of these investigations in the near future.

Acknowledgments. We are grateful for the support provided by the National Science Foundation (CMS-9500184), the National Aeronautics and Space Administration (NAG5-2774), and the Iowa Institute of Hydraulic Research. Numerical computations were performed under collaborative agreement between the Department of Geography, the Swiss Federal Institute of Technology (ETH), and the University of Iowa Institute of Hydraulic Research. We also thank Emad Habib for his help.

REFERENCES

Beard, K. V., 1977: Terminal velocity adjustment for cloud and precipitation drops aloft. *J. Atmos. Sci.,* **34,** 1293–1298.

Fujita, I., M. Muste, and A. Kruger, 1998: Large-scale particle image velocimetry for flow analysis in hydraulic applications. *J. Hydraul. Res.,* **36,** 397–414.

Habib, E., 1999: A CFD approach for efficiency assessment of rainfall measuring instruments. *Proc. John F. Kennedy Student Paper Competition, IAHR XXVIII Congress,* Graz, Austria, in press.

Hinze, J. O., 1975: *Turbulence.* McGraw-Hill, 790 pp.

Krajewski, W. F., A. Kruger, and V. Nešpor, 1998: Experimental and numerical studies of small-scale rainfall measurements and variability. *Water Sci. Technol.,* **37,** 131–138.

Larson, L. W., and E. L. Peck, 1974: Accuracy of precipitation measurements for hydrologic modeling. *Water Resour. Res.,* **10,** 857–863.

Launder, B. E., and D. B. Spalding, 1974: The numerical computation of turbulent flows. *Comput. Methods Appl. Mech. Eng.,* **3,** 269–289.

Legates, D. R., and T. L. DeLiberty, 1993: Precipitation measurement biases in the United States. *Water Resour. Bull.,* **29,** 855–861.

Marshall, J. S., and W. M. Palmer, 1948: The distribution of raindrops with size. *J. Meteor.,* **5,** 165–166.

Nešpor, V., and B. Sevruk, 1999: Estimation of wind-induced error of rainfall gauge measurements using a numerical simulation. *J. Atmos. Oceanic Technol.,* **16,** 450–464.

Sevruk, B., and W. R. Hamon, 1984: International comparison of national precipitation gauges with a reference pit gauge, instruments and observing methods. Rep. 17, World Meteorological Organization, Geneva, Switzerland, 86 pp.

Ulbrich, C. W., 1983: Natural variation in the analytical form of the raindrop size distribution. *J. Climate Appl. Meteor.,* **22,** 1764–1775.

Yang, D., B. E. Goodisson, J. R. Metcalfe, V. S. Golubev, R. Bates, T. Pangburn, and C. Hanson, 1998: Accuracy of NWS 8″ standard nonrecording precipitation gauge: Results and application of WMO intercomparison. *J. Atmos. Oceanic Technol.,* **15,** 54–67.